Verified PEMFC heavy-duty long-haul truck vehicle model with thermal management limitations of conventional cooling systems

Downloaded from: https://research.chalmers.se, 2026-11-18 14:22 UTC

Citation for the original published paper (version of record):
Boßer, C., Sedarsky, D. (2025). Verified PEMFC heavy-duty long-haul truck vehicle model with thermal management limitations of
conventional cooling systems. Applied Thermal Engineering, 280(3).
http://dx.doi.org/10.1016/j.applthermaleng.2025.128025

N.B. When citing this work, cite the original published paper.

research.chalmers.se offers the possibility of retrieving research publications produced at Chalmers University of Technology. It covers all kind of research output: articles, dissertations, conference papers, reports etc. since 2004. research.chalmers.se is administrated and maintained by Chalmers Library

(article starts on next page)

Applied Thermal Engineering 280 (2025) 128025

Contents lists available at ScienceDirect

Applied Thermal Engineering

journal homepage: www.elsevier.com/locate/apthermeng

Research Paper

Verified PEMFC heavy-duty long-haul truck vehicle model with thermal management limitations of conventional cooling systems

Christian Boßer *, David Sedarsky

Chalmers University of Technology, TechForH2 excellence center, Hörsalsvägen 7A, 412 96 Gothenburg, Sweden
Department of Mechanics and Maritime Sciences, Chalmers University of Technology, Hörsalsvägen 7A, 412 96 Gothenburg, Sweden

ARTICLE INFO

Keywords:
PEMFC
Heavy-duty
Thermal management
Vehicle modelling
Cooling system
Hydrogen

ABSTRACT

In the challenge to decarbonize heavy-duty long-haul vehicles, low-temperature proton exchange membrane fuel cell propulsion offers advantages like high efficiencies, power densities and fast refueling although challenges regarding lifetime, cost and thermal management remain. Therefore, a generic 44 t truck vehicle model with conventional cooling system has been developed in Siemens Simcenter Amesim and verified against input data from Volvo Trucks to identify its thermal limitations. Accurate identification of heat rejection limitations of conventional cooling systems enables the development of improved cooling solutions for existing vehicle platforms. The resulting model runs on average 5.8 times faster than real time and reveals severe vehicle performance losses already at 20 °C ambient temperature. A fuel cell net power derating of 46 % is required to prevent overheating at reduced velocities in a hill climb driving scenario at beginning of life conditions since the radiator can only provide about 40 % of the full load heat rejection. The model endeavors to be a representative HD truck simulation and includes details that can affect vehicle operation like braking resistors to substitute engine braking, fuel cell power-ramp rates, altitude as well as power derating of the fuel cells, traction battery and electric machines. The modular vehicle model presented here can be used as a platform for investigations of enhanced fuel cell models, degradation, improved thermal management solutions or design and control strategy studies. We present a detailed heavy-duty fuel cell truck vehicle modelling approach, its verification and results from the VECTO Long-haul and two hill climb driving cycles.

1. Introduction

In the challenge of reducing greenhouse gas (GHG) emissions from the transport sector, reductions from heavy-duty (HD) vehicles are particularly important. Heavy-duty road vehicles are responsible for over 25 % of road transport GHG emissions and over 6 % of the total GHG emissions in the EU [1]. To reduce the GHG emissions from HD transport, electrifying the drivetrain with proton exchange membrane fuel cells (PEMFC) promises high efficiency and power density [2,3]. While HD battery electric vehicles require large and heavy batteries which can reduce the effective payload capacity significantly, fuel cell electric vehicles (FCEV) can achieve long driving distances by increasing the amount of stored hydrogen with lower payload reductions. However, peak PEMFC system efficiencies of 60–65 % are achieved only at low loads and reduce to about 45 % at rated power [4–8]. The resulting high heat production which is roughly equal the gross electric power production remains a major challenge. Operating at low temperatures of only 60–80 °C or up to 90 °C for short periods requires large radiator surface areas with high air flow rates and thus cooling fan power to achieve the necessary heat rejection. Mitigation of degradation effects, reducing cost and parasitic power consumption as well as the challenging thermal management (TM) are identified as the key challenges in the development of PEMFC systems [2–4,8–11].

To replace diesel engines in HD vehicles, many truck manufacturers like Volvo Trucks [12], Daimler Truck [13], Hyundai Truck & Bus [14], Toyota [15] or Nikola Corporation [16] develop or already offer FCEV. In addition, many other companies like PowerCell Group [17], cellcentric [18], Ballard Power Systems [19] or Symbio [20] have developed high-power fuel cell systems (FCSs), some of which supply the aforementioned vehicle manufacturers. Detailed overviews of existing and planned medium- and heavy-duty FCEV can be found e.g. in [5,8].

While most HD FC vehicles are currently still under development, passenger cars (PCs) like the Toyota Mirai [21–23], Hyundai Nexo [24,25] or Honda Clarity [26] are already available on the market and experimentally investigated in literature. Because FC technologies only

* Corresponding author at: Chalmers University of Technology, TechForH2 excellence center, Hörsalsvägen 7A, 412 96 Gothenburg, Sweden.
E-mail address: bosserc@chalmers.se (C. Boßer).

https://doi.org/10.1016/j.applthermaleng.2025.128025
Received 9 June 2025; Received in revised form 5 August 2025; Accepted 21 August 2025
Available online 3 September 2025
1359-4311/© 2025 The Author(s). Published by Elsevier Ltd. This is an open access article under the CC BY license (http://creativecommons.org/licenses/by/4.0/).

Nomenclature

Abbreviations

AC	**A**ir **c**onditioning
BoL	**B**eginning **o**f **l**ife
BoP	**B**alance **o**f **p**lant
BPP	**Bip**olar **p**late
BR	**B**raking **r**esistor
COP	**C**oefficient **o**f **p**erformance
DC/DC	**D**irect to **d**irect **c**urrent
EM	**E**lectric **m**achine
EoL	**E**nd **o**f **l**ife
ETC	**E**lectric **t**urbo**c**harger
FC	**F**uel **c**ell
FCEV	**F**uel **c**ell **e**lectric **v**ehicle
FCS	**F**uel **c**ell **s**ystem
GDL	**G**as **d**iffusion **l**ayer
GHG	**G**reen**h**ouse **g**as
HD	**H**eavy-**d**uty
HT	**H**igh **t**emperature
HV	**H**igh voltage
LH	**L**ong-**h**aul
LHV	**L**ower **h**eating **v**alue
LT	**L**ow **t**emperature
LV	**L**ow voltage
MT	**M**edium **t**emperature
MV	**M**edium **v**oltage
NMC-HP	**N**ickel-**M**anganese-**C**obalt **h**igh-**p**ower
NTU	**N**umber of **t**ransfer **u**nits
PCs	**P**assenger **c**ars
PEMFC	**P**roton **e**xchange **m**embrane **f**uel **c**ell
PI	**P**roportional and **i**ntegral controller
Ref	**Ref**erence
SOC	**S**tate-**o**f-**c**harge
TCU	**T**ransmission **c**ontrol **u**nit
TM	**T**hermal **m**anagement
TRM	**Tr**ans**m**ission
VCU	**V**ehicle **c**ontrol **u**nit
VECTO	**V**ehicle **e**nergy **c**onsumption calculation **to**ol
VEM	**V**ehicle **e**nergy **m**anagement

Symbols

COP	Coefficient of performance
I	Current
$\dot{m}$	Mass flow rate
N	Number of cells
Nu	Nusselt number
P	Power
Pr	Prandtl number
$\dot{Q}$	Heat flow rate
r	(Power-ramp) rate
Re	Reynolds number
t	Time
T	Torque

Greek symbols

λ	Stoichiometry

Subscripts

air	Air
aux	Auxiliaries
bat	Traction battery
brake	Brake
cell	Single cell
compr	Compressor
cool	Coolant
EM	Electric machine
FC	Fuel cell
H_2	Hydrogen
idle	Idle
lam	Laminar
low	Lower limit
max	Maximum
ramp	Power-ramp
removed	(Heat) removal
stack	Fuel cell stack
turb	Turbulent
up	Upper limit

recently gained significant traction in HD applications [4], most of the available literature focuses on light-duty and passenger car FCEVs [27]. Operating in mostly high load highway conditions increases the requirements for thermal management systems and moreover, the requirements for HD drivetrains differ significantly from PCs, requiring higher efficiencies, durability and are more cost sensitive. But lessons learned from the lower power PC segment are the starting point of HD FCS developments [4]. A general overview of modelling approaches for FCEV and their subsystems can be found e.g. in [27] and overviews that focus on the modelling of PEMFC, FCS and FC control strategies can be found e.g. in [2,28–31].

HD FCEV simulation models can be found with different purposes like the development of energy management strategies, design optimization or thermal management investigations. To develop a generic HD truck model, existing HD PEMFC vehicle simulation models that focus on on-road vehicle design and thermal management were considered. The relevant simulation models are limited to HD FC trucks with a weight above 36 t. A selection of these truck models is summarized in Table 1.

The FCS power and battery capacity dimensioning depend on many factors and influence each other, see e.g. [33]. Battery capacities have been determined, for example, to support the thermally limited FCS in 40 °C hill climbs and further increased to reach the 25,000 h lifetime

Table 1
HD FC truck vehicle simulation model overview – BoL/EoL: beginning/end of life, *H_2 consumption unit converted based on provided data.

Weight [t]	Total FC power [kW]	Total FC heat [kW]	Battery size [kWh]	H_2 cons. [kg/100 km]	Fan power [kW]	Ref
36.6	175/275	–	183/106	7.6/7.4* (BoL)	22/31 (40 °C)	[32]
36	331	–	45	10.9*	–	[33]
49	120	–	141	10.14*	–	[34]
40	360	–	30.6	9.3 (20 °C)	–	[5]
40	–	400	–	–	22 (35 °C)	[9]
40	–	435 (EoL)	–	9.6 (20 °C)	40	[35]
40/76	230	–	50	11.2/ 22.6*	–	[6]
40	150/300	–	140/70	7.4	–	[8]
–	240	–	200	–	–	[36]
40	310	–	72	< 8	30 (30 °C)	[37]

targets, presented by Ahluwalia and Wang in [32]. Performance requirements that influence the battery size were investigated by Mayr et al. in [8] and by Paul et al. in [33]. Additionally, compensation for a lack of fueling stations was included in the battery sizing by Weiss et al. in [36]. The necessary fan power not only depends on the FCS power but also on the investigated ambient temperature and radiator frontal area. Frontal areas up to 1.3 m^2 have been investigated by Doppler and Lindner-Rabl in [9] and up to 1.2 m^2 by Linderl et al. in [10]. The design studies presented in [10] are complimented by [38–40] and eventually lead to a frontal area of 1.8 m^2 at 30 °C ambient temperature presented by Döbereiner and Steinek in [37]. Typical investigated driving scenarios are hill climbs, VECTO cycles, custom driving cycles or challenging public roads like the Brennerpass.

Besides on-road HD applications, FC vehicle models and prototypes with similar high-power have been developed for a variety of off-road HD applications like trains/trams (see e.g. [41–44]), aircraft (see e.g. [45–47]), agricultural tractors (see e.g. [48,49]) and more. These cases can differ from the operation of commercial heavy-duty long-haul (LH) trucks that mainly operate on highway missions [4]. Nonetheless, the developed FCS sizing and modelling solutions can be valuable for parametrizing and modelling of on-road HD vehicles.

From the conducted literature research some HD FC vehicle models were found that are (partly) validated or include high-power FCS models that have been validated on a small-scale system (see e.g. [6,33–36,41,43–46,49]). To the best of the authors' knowledge, only very few HD FC vehicle models include a comprehensive thermal management system consisting not only of the high, medium and low temperature cooling circuits, but also a braking resistor (BR) or retarder to substitute engine braking (see e.g. [8,10,35,36,38,40,48]). Even fewer present respective BR results (see e.g. [43,44,50,51]) and none of these evaluate impact on the operation of HD trucks and thermal management. Details about overheating protection of the FC are also seldomly reported (see e.g. [9,49]). Some references include altitude effects on the vehicle's performance by including the increased power consumption on uphill sections (see e.g. [9,32,52]). However, it is important to note that the pressure and temperature reduction caused by the elevation change can also affect the FCS and vehicle operation significantly. We are aware of one truck reference that mentions the consideration [35] and otherwise only FC aircraft models include these effects due to the nature of the application, see e.g. [45].

Here, we present a detailed 0D/1D low-temperature PEMFC heavy-duty long-haul truck simulation model developed in Siemens Simcenter Amesim and its verification. The model represents a generic HD FC truck with conventional cooling systems. Accurately identifying the limitations of a state-of-the-art conventional HD cooling systems without fitting e.g. larger or more radiators but only utilizing the available space in existing truck platforms is an important step to develop suitable improved thermal management solutions, for example, utilizing water evaporation as we presented in [53] or Wagenblast et al. in [35], Lee et al in [54] and Prabakaran et al. in [55]. Furthermore, often neglected limited FC power-ramp rates, braking resistors, power derating due to FC temperature, altitude effects as well as traction battery and electric machine power limitations are implemented and allow for a comprehensive vehicle performance and thermal limitations evaluation.

After the presented literature review of existing FC HD vehicles and simulation models in Section 1, a detailed overview of the vehicle modeling approach follows in Section 2. In Section 3, the verification and results of the full vehicle model are presented. Finally, the conclusion and outlook are presented in Section 4.

2. Fuel cell hybrid electric vehicle model

A full 0D/1D vehicle simulation model of a 6 × 2 44 t PEMFC hybrid electric heavy-duty long-haul truck has been developed in Siemens Simcenter Amesim (version 2410). The main goal of the model is to provide detailed insights into the operating conditions that FCs face under realistic driving conditions, including the complexity caused by the interdependency of the components involved. First, a general overview of the vehicle model is given in the following section. More details on the FCS modelling follow in Section 2.1, modelling of the vehicle itself in Section 2.2 and thermal management in Section 2.3. A schematic overview of the modeled FC truck is shown in Fig. 1.

To provide a general overview of the vehicle, only one of the two FCSs is shown Fig. 1 and a more detailed layout of the thermal management follows is Section 2.3. The low-temperature PEM fuel cell is connected to the powertrain via a DC/DC converter which boosts the FC voltage to the high voltage (HV) level of 800 V. It is supported by a Li-ion traction battery in transient driving operations and to recover braking energy. The battery operates at a medium voltage (MV) of around 600 V and is connected to the HV circuit via a DC/DC converter. An additional 12 V low voltage (LV) circuit and battery are implemented for the LV auxiliary devices. The electric drive train of the vehicle consists of two electric motors, a transmission and several vehicle control units (not shown, see Section 2.2.4).

To operate the FC, balance of plant (BoP) components for air and hydrogen supply are necessary. An electric turbocharger (ETC) supplies filtered air first to the humidifier and then to the FC. The hot, compressed air must be cooled in an intercooler to stay within the humidifier and FC inlet air temperature limits [45]. Hydrogen is supplied from a 700 bar tank, preheated and fed to the FC while the anode exhaust is recirculated and periodically purged. Together with the BoP the FC forms the fuel cell system (FCS). Furthermore, three cooling circuits are implemented, a high temperature (HT) circuit for the FCSs and braking resistors (BRs), a medium temperature (MT) for the powertrain and power electronics and a low temperature (LT) circuit for the traction battery. The traction battery can additionally be cooled by the cabin air conditioning (AC). The BRs dissipate heat into the HT circuit and thus substitute engine braking. Also included in the HT circuit are ion filters (electric conductivity not modelled).

To reduce model complexity, the power, heating and cooling demand of the cabin is included with other consumers like the control units and lights in a 5 kW constant power consumer. Since the focus is on the critical cooling limitations of the FC cooling system, the thermal management of the cabin itself is not further investigated. Under these conditions, the AC system is assumed to consume additional power and cabin assumed to not act as a heat sink. Furthermore, no investigations of cold start behavior are conducted in this study.

All gases are assumed to be semi-perfect, i.e. defined by the ideal gas equation with temperature-dependent properties. Initial conditions of the ambient air are defined at sea level standard conditions of 20 °C, 1.013 bar and 50 % relative humidity and it only consists of oxygen, water and nitrogen. While the temperature and pressure of ambient air change with altitude, relative humidity and mass fractions are assumed to be constant. The change in ambient conditions is determined based on the vehicle's altitude. The change in temperature is determined with the ISA standard of 6.5 °C/km, valid for altitudes below 11 km [56]. The changed ambient temperature, pressure and therefore density are used for the driving resistance calculations, the FCS air inlets and outlets as well as for the HT, MT and LT radiator-fan assemblies. Driving conditions are considered dry with no wheel slip and no wind. Constant efficiencies are used for all components, except for the FC and ETC.

2.1. Fuel cell system modelling

The developed fuel cell system model represents a generic state-of-the-art HD PEMFC system with a layout that is mainly inspired by the cellcentric stack [57] although the system is modelled as a single lumped component. Two identical and modular FCSs are implemented in parallel with individual DC/DC converters. More details on multi-stack arrangements can be found e.g. in [58]. The system is investigated at the beginning of life (BoL) and thus no effects of degradation are

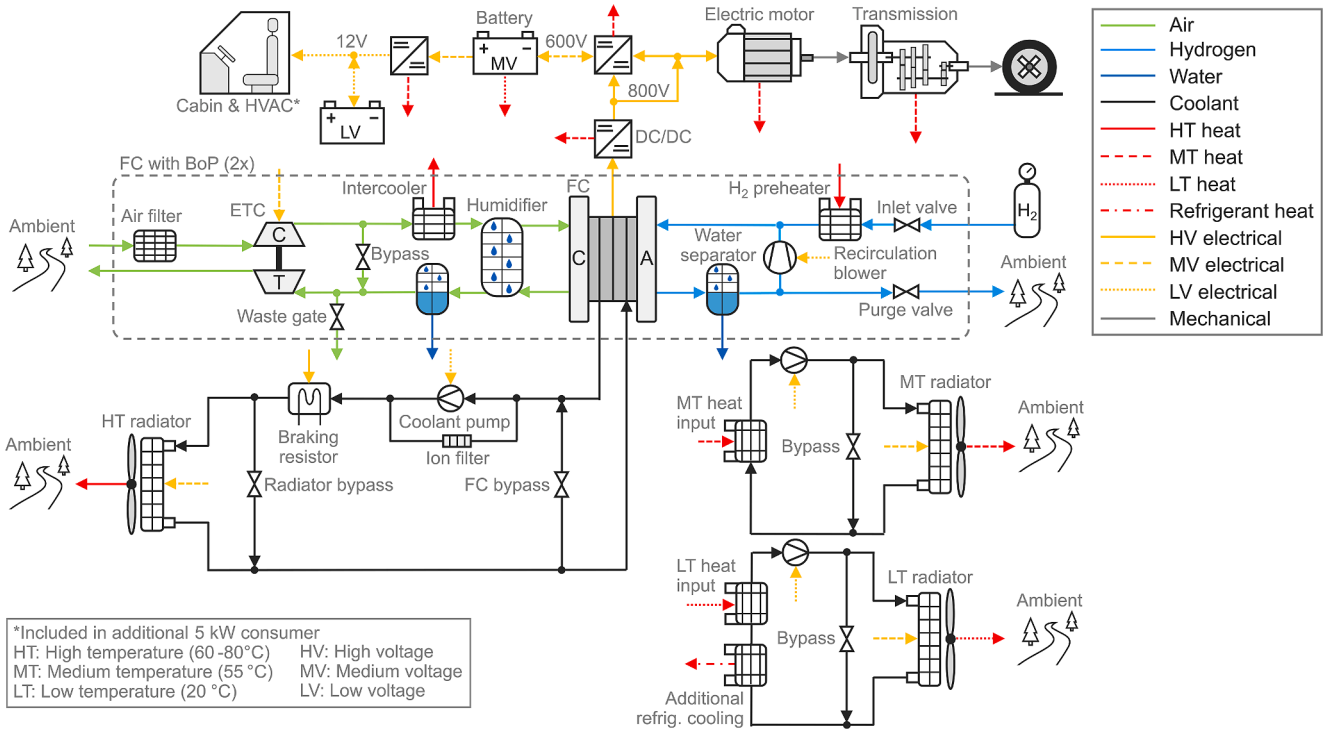

Fig. 1. Schematic fuel cell hybrid electric truck model overview.

considered. Layout and setup of the PEMFC stack model are based on the lumped modelling approach in Siemens Simcenter Amesim.

2.1.1. PEM fuel cell

A schematic overview of the FCS model can be seen in the center of Fig. 1 and the main specifications of the modeled FC stacks are summarized in Table 2 with net efficiencies based on the lower heating value (LHV) of the input hydrogen (including the BoP components, TM not included):

The total idle power is set to 30 kW which results in around 0.83 V maximum cell voltage, close to the 0.82 V voltage clipping necessary to reach the 25,000 h lifetime target found for a similar sized FCS in [32]. The FC stacks are each supplied with air and hydrogen by an individual BoP (see Section 2.1.2) and controlled by receiving an identical current request from the vehicle energy management (see Section 2.2.4). All electrochemical calculations are defined in a lumped FC stack model, while the reactant flow through the bipolar plates (BPP), gas diffusion layer (GDL) and catalyst layer as well as the heat transfer in the cooling channels are handled in separate fluid flow models. These lumped components are scaled to stack level by multiplying the single cell parameters with the total number of cells. This approach results in a uniform voltage, temperature and reactant distribution throughout the cells and stacks, neglecting spatial distributions in the stack and cell. This uniform distribution is a common approach to reduce the computational expense but also impacts the ability of the model to evaluate e.g. local hot spots, non-uniform current densities and thus performance of the individual cells [3,28,59,60], which requires further investigation in future studies to evaluate the impact on a full size stack level during vehicle operation.

The BPPs are divided into three separate flow channel components, one for air, hydrogen and coolant, respectively. Reactant and coolant channel dimensions of the BPP are calibrated to match the respective pressure drop input data from Volvo Trucks. The resulting coolant and reactant flow in the circular channels is laminar and assumed to be fully developed. For laminar flow and constant wall temperature, the Nusselt number is $Nu = 3.66$, according to Incropera et al. [61]. Since the lumped mass approach neglects temperature distributions, it is assumed that its temperature represents the average cell temperature. No conduction, convection or radiation losses through the stack casing are considered.

Amesim's PEMFC stack model is used to model the electrochemical reactions. The overall cell voltage is determined by an equivalent electric circuit model of the membrane electrode assembly, assuming a fuel utilization of 100 %. The potential at the cathode and anode is determined by the Nernst potential as a function of pressure and temperature. To determine the actual cell voltage, the voltage drop at the cathode and anode side is modelled by determining the activation losses based on the electrode double layer capacitance and the reaction current, defined by the Butler-Volmer equation. More details on the modelling approach can be found e.g. in [2,59]. Additionally, the ohmic proton resistance of the membrane is considered while the ohmic resistance of the current conductors is neglected. The proton conductive resistance is calibrated to match the fuel cell performance from Volvo Trucks' input data by assuming a fully humidified membrane, an assumption often used in simulation models [28] and considered a valid assumption if no extensive experimental data is available [31]. Heat losses are determined based on the thermoneutral potential with vapor product water (LHV) and heat of condensation in the GDL, for more details see e.g. [2,59]. The mass transport losses are represented in the form of a reduced oxygen/hydrogen supply from the BPP channels through the porous media GDL model. Oxygen, hydrogen and nitrogen diffuse through the

Table 2
Specifications of the two modelled fuel cell systems (combined).

Parameter	Value	Unit
Rated total FCS net power	328	kW
Total idle power	30	kW
Rated power net efficiency	44	%
Idle net efficiency	60	%
Max. cathode/anode gas pressure	2	bar
Stoichiometry air	1.5	–
Stoichiometry H_2	1.25	–

membrane and while oxygen and hydrogen form water, inert nitrogen is added to the anode gas mixture.

2.1.2. Balance of plant

The balance of plant (BoP) provides the fuel cell with the necessary reactants to enable the electrochemical reactions and produce electrical power for the vehicle system. The main modelled components on the cathode side are the air filter, electric turbocharger and intercooler. On the anode side, a hydrogen tank, pressure regulation valve, preheating heat exchanger and recirculation loop as well as a purge valve are modelled.

Before the air enters the FC, it is filtered to remove contaminants like sulfur dioxide, nitrous oxides and ammonia [62]. The air filters are represented by orifices to model the pressure drop at the air inlets. They are calibrated to the data provided for the MANN + HUMMEL Entaron FC 13 [63]. No ram air effects are considered for the air inlets.

The necessary air mass flow and pressure is provided by a centrifugal compressor. This compressor is part of the electric turbocharger (ETC) which consists of the electric machine (EM), its inverter and a turbine on the exhaust side including a wastegate. All components except for the turbine and wastegate are parameterized according to the Rotrex EK40CT-2429 for which the compressor pressure ratio, efficiency map and turbine backpressure line are available from the manufacturer [64]. The specifications of the modelled ETC can be found in Table 3.

The required air mass flow rate ($\dot{m}_{air}$) is determined according to Dicks and Rand [59], but adapted to use the FC stack current (I_{stack}) and number of cells (N_{cell}) as input variables:

$$\dot{m}_{air} = N_{cell} \bullet I_{stack} \bullet 3.58 \bullet 10^{-4} \bullet \lambda_{air} \quad (1)$$

with the air stoichiometry λ_{air}. The rotational speed of the map based Amesim compressor model is controlled by a PI-controller based on the target air mass flow rate. To match the operating conditions of the FC with the pressure ratio map of the compressor, a bypass has been implemented that increases the compressor air flow at low pressure ratios to avoid crossing the surge line. This bypass air stream is fed to the front of the turbine to be partially recovered and the pressure at the cathode side is controlled by opening the wastegate. At higher altitudes, the inlet pressure into the compressor reduces compared to sea level which can lead to operating conditions which exceed of the pressure ratio and speed limits. Thus, the wastegate opening pressure is adjusted to open earlier with reducing ambient pressures. A similar approach to operate the compressor has been described in [45,65]. Additionally, a minimum compressor speed has been set to avoid FC pressures below 1 bar even at idle conditions at the investigated maximum altitude of 1.4 km (see Section 3). A charge air intercooler is located after the compressor to match the cathode air inlet with the average FC cell temperature. An ideal intercooler is modelled to estimate the necessary heat removal capacity and to account for additional heat input into the HT cooling loop.

The turbine pressure ratio and efficiency map are extracted from an electric turbocharger design study at Lund University/Volvo Powertrain AB by Hansson and Abu Al-Soud for a similar FCS in [66]. The map based Amesim turbine model does not take expansion limits, condensation or backpressure into account. Therefore, an additional orifice at the turbine outlet is used to match the expected pressure recovery. The ETC is powered by an electric machine with a fixed gear ratio and liquid cooling by the MT cooling loop.

On the anode side, ambient temperature hydrogen is supplied from a 700 bar hydrogen tank to an 8 bar prechamber, compare e.g. [67]. The inlet valve controls the inlet mass flow from the prechamber by matching the anode pressure to the cathode pressure. An anode recirculation pump controls the hydrogen stoichiometry (λ_{H_2}) by adjusting the mass flow rate at the anode, each controlled by a PI-controller. The required hydrogen mass flow rate ($\dot{m}_{H2}$) is determined according to [59] as:

$$\dot{m}_{H_2} = N_{cell} \bullet I_{stack} \bullet 1.05 \bullet 10^{-5} \bullet \lambda_{H_2} \quad (2)$$

The recirculation loop is implemented to avoid waste of hydrogen and recirculate water to improve the membrane water content [59,68]. Speed, power and pressure head of the recirculation pump are parameterized similar to the SRM ARC-17 [69]. To remove accumulated nitrogen, a purge valve is periodically opened to flush the anode side [68]. The purge valve opening is determined by measuring the nitrogen molar fraction in the recirculation loop.

2.2. Vehicle modelling

The sizing and layout of the modelled truck is based on the different prototypes and design studies presented in Section 1 as well as the input data from Volvo Trucks. An overview of the truck specifications is shown in Table 4.

No packaging or sizing study has been conducted and component weights are not considered other than to specify a thermal mass that connects to the respective cooling loop. The three modelled electric circuits are connected to each other by converters that transform the power to the respective voltage level. Each converter is modeled with constant efficiency, 0.985 for the FC DC/DC converter and 0.97 for the MV and LV converter, respectively.

2.2.1. Drivetrain

The Amesim vehicle model computes the vehicle acceleration and thus velocity based on the available traction and braking power to overcome the driving resistances caused by tire friction, air drag, inclination and inertia. More details on longitudinal vehicle dynamics can be found e.g. in [71,72].

The drivetrain consists of two traction electric machines connected to a transmission (TRM) and final drive, modeled with constant efficiencies. The 12 forward gears have been parametrized according to the Volvo electric drive unit [73] but in the presented investigations only a fixed gear ratio is used to remove the influence of a shifting strategy on the results. To allow the vehicle to reach 100 km/h without shifting, the transmission is kept in 7th gear with a gear ratio of 3.44 but the final drive ratio has been changed to 5.6. Additionally, the maximum rotational speed of the electric traction machines has been set to 10,000 rpm. An overview of the modelled traction EM and transmission specifications is shown in Table 5.

The EM specifications have been adapted from the Daimler GenH2 truck [74]. EMs similar to the modelled ones are also implemented e.g. in [37,75]. The specified drivetrain results in an efficiency of 84 %.

Table 3
Modelled ETC specifications, based on the Rotrex EK40CT-2429.

Parameter	Value	Unit	Ref
Max. compressor speed	120,000	rpm	[64]
Max. motor speed	16,000	rpm	[64]
Compressor gear ratio	7.5	–	[64]
Continuous/peak motor power	40/60	kW	[64]
Motor and inverter efficiency	0.95	–	

Table 4
Specifications of the modelled truck.

Parameter	Value	Unit	Ref
Total vehicle mass	44	t	[70]
Frontal area	9.7	m^2	[5]
Drag coefficient	0.48	–	
Rolling resistance coefficient	0.0045	–	
Wheel radius	0.507	m	[5]
Wheel inertia	15.5	kgm^2	[5]
Number of wheels front	2	–	
Number of wheels rear	8	–	

Table 5
Specifications of the modelled transmission and a single traction electric machine incl. inverter.

Parameter	Value	Unit	Ref
Traction EM peak power	330	kW	[74]
Traction EM continuous power	230	kW	[74]
Traction EM peak torque	2,071	Nm	[74]
Traction EM efficiency	0.95	–	[5]
Traction EM inverter efficiency	0.95	–	
Transmission gear efficiency	0.98	–	[5]
Final drive efficiency	0.95	–	[5]

2.2.2. 600 V Li-ion traction battery

The 600 V Li-ion traction battery in the MV circuit is used as a buffer for the limited transient performance of the FC stack and to recover energy from regenerative braking. The Amesim battery pack model uses an equivalent circuit model including ohmic losses from charge and discharge currents, for more details see e.g. [71]. Open circuit voltage curves, ohmic resistances and cell capacities are available in the Amesim database of validated battery cells from which a Nickel-Manganese-Cobalt high-power (NMC-HP) cell was chosen for the model powertrain. The usable state-of-charge (SOC) range of the battery is limited to 10–90 % to prevent the exceedance of voltage limitations. No degradation effects are considered, and the implemented battery specifications can be found in Table 6.

The heat transfer from the lumped battery mass to the LT coolant is modelled with the thermal conductance of a thermal interface material identified by Ramesh Babu et al. in [76]. It is assumed that this interface material has the highest thermal resistance between the cells and the coolant and thus the convective heat transfer resistance to the coolant is neglected. Additionally, the density, heat capacity and thermal conductivity of the bulk battery material are adapted from [76]. The battery casing is assumed to be well insulated and thus its heat rejection is neglected.

2.2.3. Braking resistors

Due to the electric drive train architecture, a substitute for engine braking is required. To avoid brake fading in downhill sections and in repetitive deceleration events, the electric traction machines regeneratively brake the truck. This electric power can recharge the traction battery, but only to the maximum power and charge limitations of the battery [40,77]. To dissipate the remaining electric power as heat into the HT-cooling loop, two braking resistors are connected in series to the FC. This series connection allows for an increased coolant temperature into the radiator and thus improved heat rejection. The combined specifications of the implemented BRs are shown in Table 7.

The two braking resistors are connected in parallel to each other and have been parameterized similar to the specifications of the Danotherm WHBSA 200 series [78], adjusted to the specific HT cooling system limitations.

2.2.4. Vehicle energy management and control units

The vehicle is controlled by a set of control units that coordinate the power supply to the wheels and the power distribution between the traction battery, fuel cell and braking resistor. Overviews of how energy management strategies (EMS) can be realized and optimized can be found e.g. in [5,52,77,79]. In this study, a supply and demand EMS without predictive control or prior route information is implemented to investigate the vehicle operation. A schematic overview of the vehicle energy management and control unit structure is shown in Fig. 2.

Table 6
600 V Li-ion traction battery specifications.

Parameter	Value	Unit	Ref
Number of cells in series	163	–	
Number of cells in parallel	7	–	
Pack capacity (at 3.7 V, gross)	34.4	kWh	
Thermal interface material resistance	0.004252	m^2K/W	[76]

Table 7
Specifications of modelled braking resistors (combined).

Parameter	Value	Unit	Ref
Max. power (10 sec every 60 sec)	350	kW	
Continuous power	200	kW	
Maximum coolant pressure	3	bar	[78]
Coolant pressure drop	0.2–0.5	bar	[78]

The target velocity and road gradient of a respective driving cycle are defined in the forward controlled Amesim driver component. This driver model uses a model-based control that compares the predicted vehicle velocity to the target velocity based on an internal vehicle model. The velocity dependent maximum acceleration and deceleration are limited to the default limits of the VECTO cycle database (version 3.3.10.2401, more details see [80]). They are used to represent a realistic driver behavior compared to using the maximum available power of the EM and brakes in each acceleration and deceleration event.

The driver command is sent to the Amesim transmission (TCU) and vehicle control unit (VCU) model in form of an acceleration, braking and gear request signal. From the VCU, the braking torque (T_{brake}) is sent to the brakes. To control the torque of the traction electric machines (T_{EM}), the VCU requires an upper ($T_{EM,up}$) and lower torque limit ($T_{EM,low}$) input. Therefore, a vehicle energy management (VEM) control unit has been developed to control the power distribution between FC (P_{FC}), traction battery (P_{bat}) and BRs (P_{BR}) based on these limits.

Thus, the VEM has three main objectives during driving and braking: (1) determine how much power the FC stacks need to produce, (2) convert the power limitations of the traction battery, EMs and BRs into an upper and lower torque limit of the EMs and (3) determine how much power is dissipated as heat in the BRs. The determined torque limits directly control the driving and regenerative braking power (P_{EM}) which indirectly limits the battery charge/discharge and BR power. In case the battery SOC drops to 10 %, the controller prevents any further discharge of the battery. Instead, the maximum EM input power is limited to the remaining power of FCSs minus all auxiliary consumers (P_{aux}). The FC controller as well as the time-based peak and continuous power controller are modelled within the VEM.

At sufficiently high battery SOC, the FC power request follows the required traction EM power within the limits of the available FC power. To reduce degradation effects in dynamic operation and avoid rapid load changes that could cause insufficient reactant supply, see e.g. [49] or [81], the FC power-ramp rate is limited (r_{ramp}):

$$\left|\frac{dP_{FC}}{dt}\right| \leq r_{ramp} \tag{3}$$

All auxiliary power, including the BoP, is provided by the FC. If the SOC of the battery reduces to 30 % and the FC has the capacity to provide more power than the EMs request, the battery is charged (P_{bat}) until the SOC reaches 60 %. This leaves available battery capacity for regenerative braking, compare e.g. [9]:

$$P_{FC} = P_{EM} + P_{bat} + P_{aux} \; with \; P_{FC,idle} \leq P_{FC} \leq P_{FC,max} \tag{4}$$

The lower limit of the FC power is defined by the idle power ($P_{FC,idle}$) and the upper limit ($P_{FC,max}$) depends on the limitations of the cooling system. In case the FC coolant outlet temperature exceeds a maximum temperature of 84 °C, the FC power is derated by a temperature PI-controller that reduces the maximum FC power to maintain a coolant outlet temperature of 82 °C, matching the FC heat load with the heat rejection capabilities of the radiator. The temperature derating is turned off and the regular FC control takes over if the temperature reaches the setpoint of 78 °C again. This temperature hysteresis is implemented to avoid overshooting and oscillation in the temperature derating

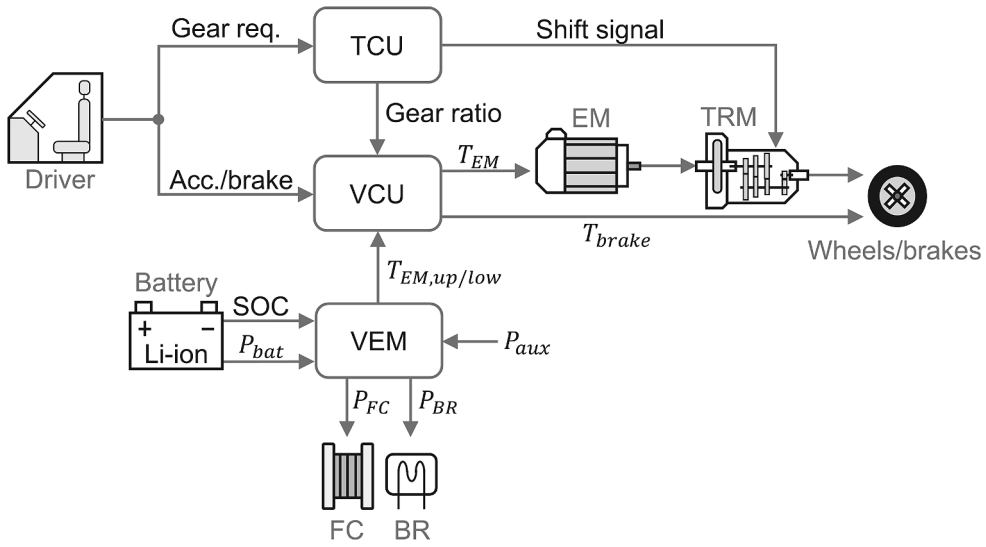

Fig. 2. Schematic overview of vehicle energy management and control units.

controller.

The time-based control is used to simplify the control of peak and continuous power in a state-chart controller instead of using detailed temperature control models for the traction battery, EM and BR. The time limit for peak power of the traction battery and EM is 30 s, based on the provided Amesim battery data and [8], for the BR the time limit is set to 10 s based on [78]. If this duration is exceeded, the limit is reduced to the continuous power limit and a necessary cooldown time of 30 s (60 s for the BR [78]) is assumed. To avoid oscillations and saw profiles, an additional lower threshold is used.

2.3. Thermal management modelling

To maintain the required operating temperature of the propulsion system, waste heat is rejected to the ambient air by individual radiators in each cooling loop. Main focus is set on the HT cooling investigations, but basic MT and LT cooling loops are integrated to capture additional power consumption and heat rejection requirements. The radiator fan assembly in the front of the vehicle is dedicated to the HT circuit, cooling the two FC stacks and the BRs. To avoid obstructing the HT radiator, one radiator fan assembly each for the LT and MT cooling loop is located in the side panels behind the driver cabin. Side panels have for example been implemented in the Mercedes-Benz GenH2 prototype truck [13]. Alternative vehicle and thermal management layouts can be found e.g. in [10,35,37]. The MT loop is dedicated to the traction EMs, the converters as well as the transmission, and the LT loop to the traction battery. All cooling loops use a 50/50 mixture of water and ethylene–glycol as a coolant and all pipes are modelled as perfectly insulated. Components that are not connected to a cooling loop are assumed to be passively air cooled.

2.3.1. Fuel cell (HT) cooling

The two FCSs in the HT cooling loop are connected in parallel and receive the same coolant mass flow and inlet temperatures. Because the HT circuit has the highest heat rejection capacity, it also cools the braking resistors. An overview of the modelled HT cooling loop layout is schematically shown in Fig. 3.

In addition to the FC stack in the primary circuit (black solid line), the HT loop also preheats the injected hydrogen gas and cools the charge air in the secondary circuit (black dashed line) to stack temperature.

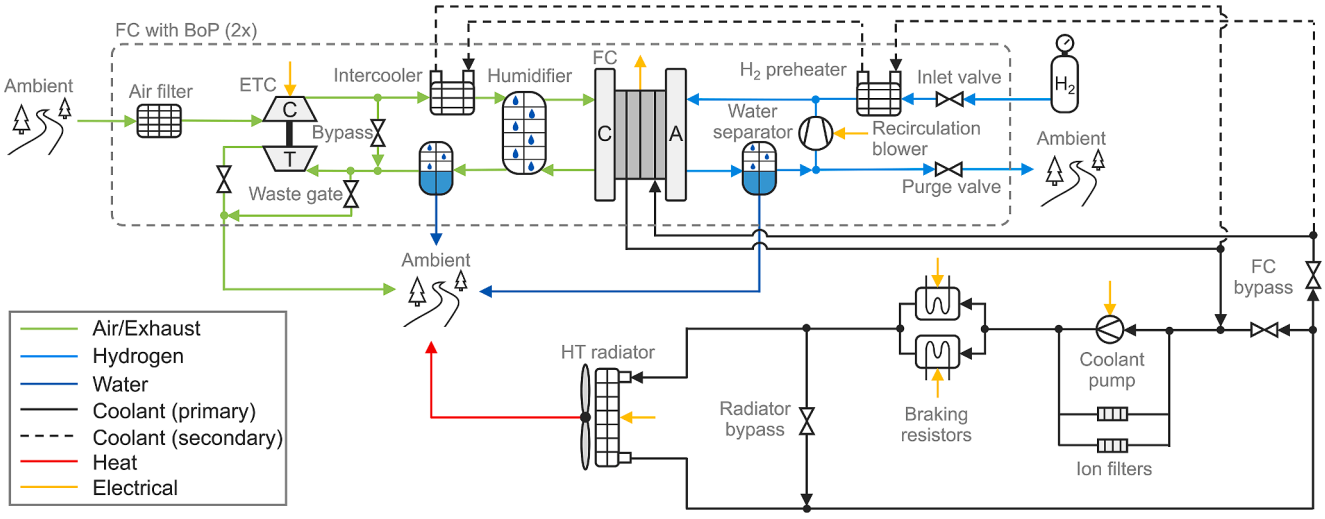

Fig. 3. Schematic HT cooling layout.

Two ion filters are connected in parallel to the coolant pump to deionize the coolant. These are modelled as flow restrictions (conductivity not modelled). The ion filter pressure drop is calibrated to the MANN + HUMMEL OmniFlow i6-3 [82].

The coolant pump has been parameterized to the EMP WP150 HV electric water pump specifications with a maximum power consumption of 3 kW [83]. The coolant pump speed is controlled by a PI-controller based on a fixed ratio to the FC and BR power and thus heat generation. This control does not minimize the coolant pump power consumption but has the advantage that the coolant pump directly responds to increases in heat generation instead of reacting to a delayed coolant temperature increase at the FC or BR outlet. To precisely control the FC stack temperature, a FC and radiator bypass are implemented. The FC bypass controls the coolant flow to the FCS to maintain a target FC outlet temperature of 78 °C even if the use of the BR requires high coolant flow rates, e.g. during downhill braking with idling FC. The radiator bypass on the other hand ensures a FCS inlet temperature of 60 °C even if the radiator outlet temperature is below the setpoint. This can occur due to the ram air flowing through the radiator even if the fan is turned off. Since the coolant pump is not controlled by the FC inlet or outlet temperature, potentially oscillating behavior from multiple controllers acting on the same input is prevented. Improvements could be achieved by using advanced control strategies like model predictive control, compare e.g. [84]. If the heat generation exceeds the heat rejection capabilities of the radiator, e.g. at full load over longer periods, the FC temperature derating controller described in Section 2.2.4 is activated to prevent overheating of the FC.

According to the component requirements for the ion filter [82] and BR [78], the upper limit for the coolant pressure must not exceed 3 bar. Furthermore, high pressure differences between the reactant gas and coolant side in the BPP of the PEMFC need to be avoided to prevent mechanical damage of the cell (not modelled). According to Nöst et al. [85], the pressure difference should be below 50 kPa. Both limitations are respected in the implemented model without extra measures for most of the vehicle operation.

The Amesim radiator-fan assembly model is used for the ram air effect and underhood flow through the cooling system. A grille with an open area ratio of 0.75 and depth of 0.05 m covers the air inlet into the radiator. Due to the driving velocity of the vehicle, the ram air effect can create enough pressure in front of the grille to overcome the pressure losses through the grille and radiator to cause an air flow (see e.g. [86]). The conversion from dynamic to static pressure at the radiator grille inlet and low-pressure underhood zone at the fan outlet is modelled with constant pressure coefficients.

A crossflow plate-and-fin radiator with a frontal area of 0.9 m^2 is implemented for the HT cooling loop. To maximize the heat rejection, the largest depth of 0.143 m for typical truck radiators found by Doppler and Lindner-Rabl, in [9] and a dual pass configuration are used. The geometric parameters and heat transfer capabilities have been adjusted to the experimental results from Prabakaran et al. [55], who provide extensive geometric and experimental data for the investigated small-scale dual pass radiator for water spray cooling in FCEV applications. Since these investigations focus on automotive FC applications, the investigated air flow rates, temperatures and velocities as well as coolant temperatures are in close match with the operating range for the presented vehicle model in this study. An overview of the modelled HT radiator specifications is shown in Table 8.

Table 8
Specifications of modelled HT radiator.

Parameter	Value	Unit	Ref
Free flow area / frontal area coolant side	0.206	–	[55]
Free flow area / frontal area air side	0.653	–	[55]
Radiator width	1	m	
Radiator height	0.9	m	
Radiator depth	0.143	m	[9]
Hydraulic diameter coolant side	3.1	mm	[55]
Hydraulic diameter air side	1.57	mm	[55]
Number of channels per pass	61	–	

The small-scale radiator has been modeled in Amesim, validated against the provided measurement data and then scaled up to the required dimensions. It is modelled with the effectiveness-NTU method, for more details see e.g. [61]. The correlations for the Nusselt number (*Nu*) for air and coolant flow for laminar and turbulent regimes have been determined with the Amesim "Heat Exchange Regression Tool" which fits the Nusselt correlations to the provided measurement data.

The laminar Nusselt number for the coolant flow results in:

$$Nu_{lam,cool} = 0.2498 \bullet Re^{0.4197} \bullet Pr^{0.3333} \quad (5)$$

The laminar Nusselt number for the air flow results in:

$$Nu_{lam,air} = 0.0436 \bullet Re^{0.7029} \bullet Pr^{0.3333} \quad (6)$$

The turbulent Nusselt number for the coolant flow results in:

$$Nu_{turb,cool} = 0.0038 \bullet Re^{1.128} \bullet Pr^{0.3333} \quad (7)$$

The turbulent Nusselt number for the air flow results in:

$$Nu_{turb,air} = 0.04 \bullet Re^{0.7019} \bullet Pr^{0.3333} \quad (8)$$

with the Reynolds number *Re* and Prandtl number *Pr*. The temperature change of the coolant flow through the dual pass is partly modelled by determining the average coolant temperature per pass and which is used to determine the heat transfer to the air. The peak heat exchanger effectiveness for the HT is around 0.93. Radiative heat losses are neglected.

When the ram air flow is not high enough to achieve the target radiator coolant outlet temperature of 60 °C, a fan is used to increase the air flow rate. The respective mass flow rate and pressure drop over the individual components is determined based on the fan speed. The fan is controlled by a PI-controller based on the radiator coolant outlet temperature. To model the fan, the volume flow rate curve of a 400 mm fan has been adapted from the Gamma Technologies GT-SUITE (v2023) "Fuel_Cell_Truck-Flow" example. It is scaled up with the fan affinity laws (see e.g. [87]) to an 850 mm fan and the isentropic efficiency is set to constant 30 %. Due to noise level restrictions, the maximum speed of the fan is limited to 1500 rpm.

2.3.2. Traction battery (LT) cooling

To capture the additional heat load and power consumption of the traction battery thermal management, a low temperature cooling loop with reduced complexity is implemented. Simplifications are made regarding the heat transfer from the battery to the coolant (see Section 2.2.2), the coolant pump control and the vapor-compression cycle.

The LT coolant pump is parameterized with the same flow map as the HT coolant pump, scaled to a smaller pump diameter with the affinity laws (see e.g. [87]). It is kept at a constant speed of 4000 rpm to ensure sufficient heat removal and reduced control complexity. The same validated radiator model as for the HT cooling loop has been used but scaled to different dimensions of 1 × 0.5 × 0.05 m. The LT radiator is located in the side panel behind the driver cabin. Two fans are used to create air flow through the radiator which are parameterized with the same flow curve as the HT fan but at the reference diameter of 400 mm. The fan dimensions are close to the EMP FiC-15 HV Electric Fan [88] from which the maximum power of 3 kW has been adapted. The fan speed is PI controlled and limited to 3000 rpm. The ram air effect and low-pressure zone behind the fan are neglected, thus the air enters and leaves the grille-radiator-fan unit at ambient air conditions according to the respective altitude.

The radiator bypass operates in the same way as in the HT loop but with a setpoint of 20 °C. Additionally, it stops the coolant flow through the radiator if the ambient air temperature exceeds 21 °C to avoid warming up the coolant above the setpoint. Since the ideal operating

temperature of Li-ion batteries ranges from 15 to 35 °C [89], the heat rejection from the radiator alone cannot provide sufficient cooling, especially at elevated ambient temperatures. To cool the battery, the vapor-compression refrigeration cycle of the cabin AC system is utilized, compare e.g. [10,35] or [90]. For the model presented in this study, a simplified representation is implemented (compare Fig. 1). Before the coolant enters the battery cooling plate, it is cooled or heated to 21 °C. Since cold climate conditions are not investigated and heat could be integration from the HT or MT cooling loop (compare e.g. [10]), heating of the coolant is neglected. The cooling to the target temperature on the other hand requires additional power for the AC compressor and is modelled by using the coefficient of performance (*COP*):

$$COP = \frac{\dot{Q}_{removed}}{P_{compr}} \tag{9}$$

with the heat removed from the coolant $\dot{Q}_{removed}$ and the necessary compressor power P_{compr}. A constant COP of 1.8 is adapted from [90].

2.3.3. Power electronics, electric machine and transmission (MT) cooling

As for the LT cooling loop, the main goal of the MT cooling loop is to capture the additional heat load and power consumption. Thus, the cooling loop and the thermal model of the individual components are simplified, i.e. only lumped masses with ideal heat transfer to the coolant and no details regarding internal heat generation of e.g. electric machine windings or transmission gears are implemented. The MT cooling loop includes the two traction EMs, the transmission, the LV and MV converter as well as the FC DC/DC converter and ETC in the BoP. The two traction EMs and BoP systems are each connected in parallel and in series with the other components. This reduces complexity but does not represent accurate inlet and outlet temperatures or pressure drops in each of the components (compare e.g. [10]). The cooling loop is built identical to the LT cooling but without the AC system integration, a higher radiator outlet target temperature of 55 °C and a constant pump speed of 2900 rpm.

In the next section, the verification of the developed model and the resulting impact of the thermal management on the vehicle performance are evaluated.

3. Verification, results and discussion

The developed full vehicle model is run on an Intel ® Core™ Ultra 7 155H (1.40 GHz) processor with 32 GB ram in Siemens Simcenter Amesim version 2410. It takes on average 0.17 s computation time per simulated second or 8.7 s computation time per simulated kilometer. The computation time varies with a factor of about 0.6–2 depending on how transient the driving cycle is. In the following section, the verification results on a hill climb and the VECTO Long-haul cycle as well as the results of the altitude effects on the Brennerpass driving cycle are presented and discussed.

In the first verification step, the peak power of relevant components and the behavior of the FCS have been verified against reference data from Volvo Trucks. Because the layout, specifications and performance of the developed generic vehicle model are not identical to the Volvo Trucks prototype, comparing the simulation results to raw prototype measurement data would result in an invalid comparison. Therefore, in the second step, the full vehicle model has been verified against a validated Volvo Trucks simulation model that has been adjusted to the

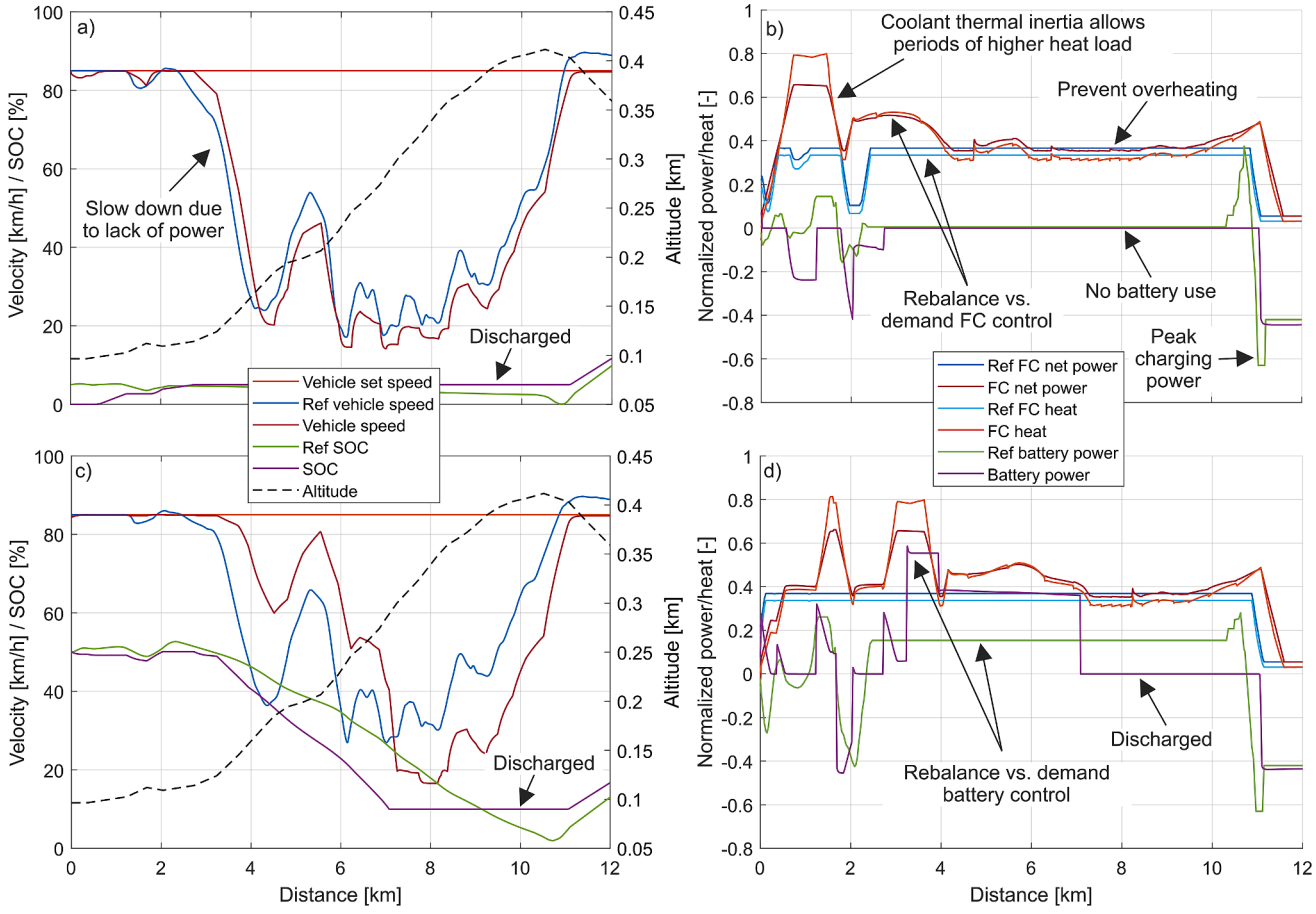

Fig. 4. Hill climb verification with depleted battery (a,b) and 50 % starting SOC (c,d) (20 °C ambient).

specifications of our generic model, i.e. radiator dimensions, FC and EM power, etc. Nevertheless, three main differences between the models remain: (1) while our model uses the previously described supply and demand strategy (see Section 2.2.4), the reference model rebalances the energy demand with prior route information, (2) our model includes the thermal mass of the coolant and (3) a different thermal management layout has been implemented in our model, including the described side panel radiators.

The vehicle model has been verified in three steps: (1) A hill climb driving cycle with depleted battery to focus on the FCS operation and limitations, (2) the same hill climb scenario with 50 % starting SOC and (3) the VECTO Long-haul driving cycle. The results of the hill climb driving scenario are shown in Fig. 4.

The hill climb scenario in Fig. 4 shows the A-30 highway between Murcia and Cartagena in Spain at 20 °C ambient temperature. In step (1), the velocities with depleted battery in diagram (a) match well and a significant slowdown of the vehicle due to insufficient power can be seen. In diagram (b), the difference between the two operating strategies and the effect of including thermal inertia can be seen from the behavior of the FCS net power and heat load. The FC in our model is controlled to follow the power demand while the reference model determines a thermally limited maximum FCS net power for the cycle. Due to the coolant inertia, the FCS in our model ramps up to a higher power for a short period before the coolant exceeds the temperature limits. The FC

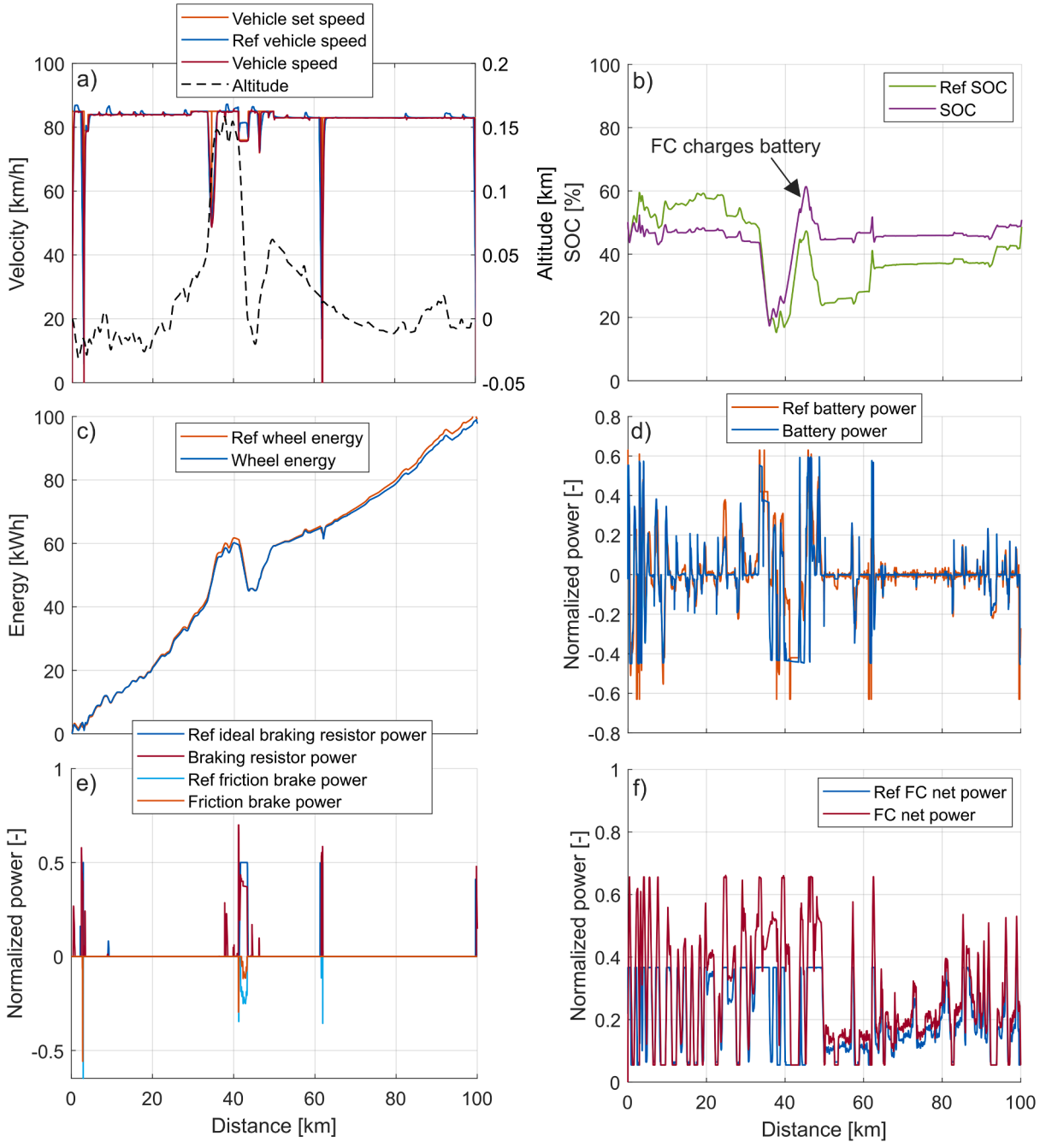

Fig. 5. VECTO Long-haul verification (20 °C ambient).

power in our model is then derated to avoid overheating, verifying a well matching FCS net power and heat load of both models. A significant FC net power derating of about 46 % at these BoL conditions is necessary in our model during this hill climb since the radiator can only provide about 40 % of the necessary full load heat rejection at the reduced velocity.

In step (2), the same hill climb scenario with 50 % starting SOC, the velocity trends of both models match well in diagram (c) while the traction battery behavior differs during the hill climb itself, shown in diagram (d). Before the vehicle starts to ascent, the battery power and SOC of both models are matching well but during the hill climb the difference between the control strategies becomes apparent for both the FC and battery. In the reference model, the battery depletion is matched with reaching the top of the hill while our model does not include prior route information and the power is supplied as requested. Additionally, only peak discharging but no peak charging power are implemented in our model and no battery usage is allowed below 10 % SOC. The FC in our model behaves similarly to diagram (b) but due to the initial support from the battery, higher velocities allow for temporary higher heat rejection before its power is derated to a similar level as for the previous case.

In step (3), the two simulation models are compared in the VECTO Long-haul cycle. The results for this 100 km highway cycle are depicted in Fig. 5.

In diagram (a), the close match of the vehicle velocities can be seen. Diagram (b) and (d) show matching trends of the battery SOC and power, except for the peak charging power included in the reference model and a different strategy regarding battery charging by the FC in our model. Thus, the battery utilization modelling is verified even though the benefits of prior route information are neglected. Diagram (c) shows well matching wheel energy between the two models and verifies accurate modelling of the driving resistances. In diagram (e), matching trends in braking resistor (different BR integration in reference model) and friction brake power are visible. Finally, in diagram (f), the FC net power is compared. As elaborated previously, the modelling and control differences allow for short periods of higher FC power in our model but in the second half of the cycle both FCS closely follow the total power demand of the vehicle. The higher FC power in our model in this section shows that the total auxiliary power demand is higher than in the reference model.

The peak power of the HT cooling fan is about 11 kW with noise limitations preventing the increase of the fan speed for increased heat rejection, resulting in a lower fan power consumption than identified in design studies to overcome the thermal limitations like [9,10] or [32]. The MT cooling loop, a peak heat rejection of around 45 kW requires around 4 kW power from the two fans. In the LT loop around 5 kW of heat is rejected by the AC system and 2.5 kW from the radiator, respectively. The battery temperature is kept below 35 °C for most of the driving cycle with a short term peak still below 38 °C. This requires an additional maximum power of 2.8 kW from the AC compressor and around 4 kW from the two fans. The additional heat load and AC compressor power consumption are verified against Volvo Trucks' input data. Further refinement in future studies, like modelling EM winding temperatures or detailed traction battery cells, would give more insights into their thermal limitations and allow for more accurate peak power limitations compared to the time-based control.

Table 9
Verification overview VECTO Long-haul (20 °C ambient).

Parameter	Unit	Ref model	Results
Average velocity	km/h	79.7	79.3
Wheel energy	kWh	98.8	95.9
Positive wheel energy	kWh	132.6	130.8
Positive wheel energy per km	kWh/km	1.32	1.31
Negative wheel energy	kWh	33.8	34.8
Battery energy	kWh	2.3	−5
Positive battery energy	kWh	35	31.6
Negative battery energy	kWh	32.7	36.7
Braking resistor energy	kWh	8.6	10.5
H_2 consumption	kg/100 km	7.1	10.3
FC net energy production	kWh	123.9	169

The driving resistances, braking resistor, friction brake and battery utilization shown in the investigated driving cycles and Table 9 match well between the reference and developed model and are thus verified.

The negative battery energy in Table 9 represents a higher final than initial SOC. The H_2 consumption of 10.3 kg/100 km in our model is about 45 % higher than the 7.1 kg/100 km in the reference model which can be explained by three effects: First (1), due to the supply and demand control of the FC and the inertia of the coolant in our model, the FCS is often running at high power for short periods which increases its losses since e.g. the FC heat load and power consumption of the cooling fan are non-linear. The FC control strategy also does not have prior information about upcoming uphill or downhill sections and charges the battery if possible (regenerative braking is prioritized). Prior route information could improve hydrogen consumption and vehicle performance once safe vehicle operation is ensured, including sufficiently high uphill speeds and downhill braking which are directly impacted by the thermal management. Different energy management strategies have been presented e.g. in [5,52,77] or [79]. Second (2), the different designs of the MT/LT cooling loops, additional consumers and drivetrain layout lead to increased power consumption in our model. Third (3), despite similar peak power consumptions of the individual components, the overall power consumption and losses of some components might be higher. A comparison of the models has shown that no single loss or power consumption stands out but distributed higher power consumptions increase the overall energy consumption. Excessive tuning of the model would be counterproductive for creating a generic vehicle model and thus no adjustment to individual components was attempted. Nevertheless, the hydrogen consumption remains consistent with the literature and prototype data presented in Section 1. The average FCS efficiency of 53 % in the VECTO Long-haul driving cycle matches well with reported FCS average efficiencies of around 50 % in e.g. [5,8,9,34].

An overview of the net energy distribution in the VECTO Long-haul cycle is depicted in Fig. 6 for the FC and BoP.

Chart (a) shows the energy distribution within the PEMFC based on the total hydrogen energy input (LHV), resulting in 55.8 % of the energy being converted into usable electricity. 42.9 % are rejected as electrochemical heat losses into the HT cooling circuit. About 1.1 % is lost in purging and 0.1 % in hydrogen crossover. The simplified purging strategy which is based on the simulated gas fractions in the anode flow is not optimized to reduce the hydrogen consumption but to balance purging intervals and cell voltage drop. Hydrogen losses with a purging strategy based on ampere hours produced by the FC stack was experimentally investigated by Reithuber et al. in [91]. It resulted in a decreasing share of hydrogen crossover and combined crossover, drainage and purging losses with increasing current densities. The respective shares on the hydrogen input were found to decrease below 1 % and 3 %, respectively, for current densities above 0.6 A/cm^2. Similar results have been obtained in this study with average current densities of 0.66 A/cm^2 in the VECTO Long-haul cycle.

Chart (b) shows the distribution of used energy in the BoP of the FCS. With about 40 kW total peak power for the two ETCs, most of the energy is expended in the ETC (66.1 %), followed by the HT FC thermal management (total 21.9 %), losses in the DC/DC converter (9.9 %) and recirculation pump (2.1 %). The overall vehicle efficiency can be determined by the share of positive driving energy on the total hydrogen LHV input, resulting in 38.1 %.

Additionally, the vehicle is investigated in a 520 km driving cycle on the Brennerpass, shown in Fig. 7. At the highest altitude of the driving cycle (around 1.4 km), the ambient temperature reduced to around 11 °C and the ambient pressure to around 0.86 barA, see diagram a).

The slowdown due to insufficient power shown in diagram a) is

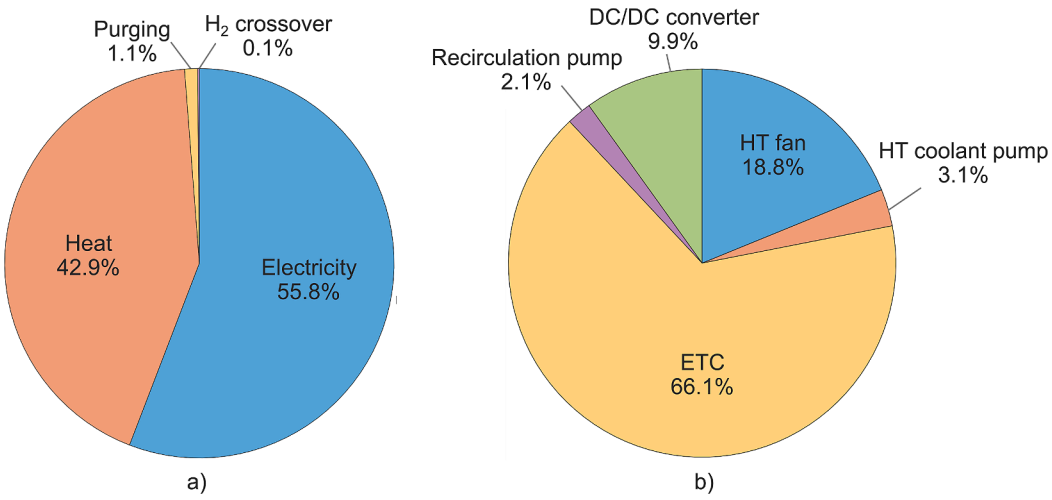

Fig. 6. Net energy distribution (based on H_2 LHV) in VECTO Long-haul (a) FC, (b) BoP.

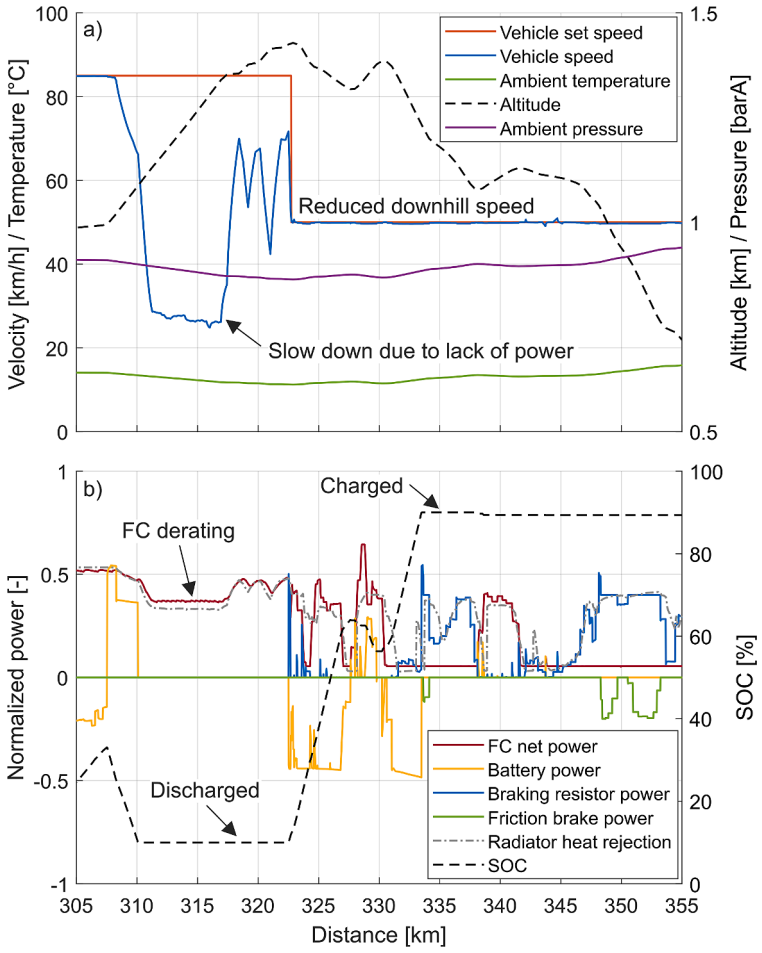

Fig. 7. Brennerpass peak altitude results.

caused by the temperature limit derated FC power and discharged battery shown in diagram b). To ensure sufficient slowdown capabilities in the downhill section, limited by the BRs, the vehicle velocity is reduced to 50 km/h. The battery reaches its charging limits before the end of the downhill section and thus cannot further support slowing down the vehicle. Therefore, the friction brakes must be applied on the three shown occasions. The heat load at the radiator is either caused by the FC, the BR or the overlap of the FC power ramp down and BR heat dissipation which increases the total heat load on the HT cooling circuit and thus a limits the maximum BR power further. Compared to more than 350 kW continuous engine braking in, for example, a Volvo D13 [92,93], the impact on the vehicle performance from to the thermal

limitations of the HT cooling circuit becomes apparent also during downhill driving.

With increased altitudes further impacts on the vehicle are identified. At the HT radiator, the heat rejection rate is not impacted since the reduced ambient temperature compensates for the reduced air flow caused by the lower air density. At the ETC on the other hand, the reduced inlet pressure leads to higher pressure ratios required to reach the same FC pressure. To avoid crossing the surge line of the compressor, the target outlet pressure is continuously reduced (see Section 2.1.2). No ram air effect for the compressor is considered but could improve its operating range. Exceeding a certain altitude would ultimately exceed the modelled ETC's capability to provide a minimum of 1 bar FC pressure, reducing the FC performance. At this altitude and the thermally derated FC operating point, it reduces the compressor outlet temperature and therefore heat load in the intercooler by 10 and 20 %, respectively. It also reduces the FC pressure by 0.3 bar compared to sea level conditions. With the current GDL parametrization of the FC model which has been calibrated with sea level inlet conditions, this pressure reduction does not result in a significant change in the cell voltage. Lower pressure would also affect the membrane humidification due to the reduced relative humidity of the inlet air [59]. Refined water management and membrane humidification modeling in future studies, including flooding effects (see e.g. [2]), could enhance the evaluation of FC performance and the impact of the thermal management during vehicle operation. Both effects could increase the heat load and thus lead to further derating of the FC. Further reduced vehicle velocity caused by the reduced FC power would in turn lead to further reduced heat rejection capabilities of the radiator. Therefore, enhanced FC models are currently developed within the research group to include refined water management and spatial distributions over stack and cell. This would enable further analysis of the fuel cell performance and the integration of degradation mechanism, defined by these local conditions. Increased heat production at the end of life due degradation in turn increases the requirements on the cooling system further [11,35,94].

4. Conclusion and outlook

The modelling and verification of a 44 t EU low-temperature PEM fuel cell heavy-duty long-haul truck has been presented. A fast simulation model was developed that performs on average 5.8 times faster than real time and focuses on the limitations that HD PEMFC trucks with conventional cooling systems face. The model includes three cooling loops and often neglected braking resistors, FC power-ramp rates, altitude effects as well as battery and electric motor power limitations.

The derived model has been verified against input data and a validated simulation model from Volvo Trucks, matching well in driving resistances, battery, braking resistor and friction brake utilization as well as heat rejection limitations. In terms of total energy consumption, a different vehicle layout and control strategy lead to a deviation in hydrogen consumption, although still consistent with literature data. Improvements could, for example, be achieved with energy management strategies that include prior route information. At higher altitudes, the lower ambient temperature compensates for the reduced density in the radiator, but the FC turbocharger is affected if designed for sea level inlet conditions, reducing the FC operating pressure. Further refinement is necessary for the FC model to capture detailed water management, mass transport and non-uniformities over cell and stack.

The results presented here demonstrate accurate modelling of the thermal limitations of conventional cooling systems in HD FCEV, especially in the worst case scenario of a hill climb with depleted battery as this is the most challenging scenario for the thermal management. This scenario shows the significant impact that the thermal management has on the vehicle performance. The maximum FCS net power in our model requires a power derating of about 46 % already at 20 °C ambient temperature and BoL conditions to avoid overheating during a low velocity hill climb since the radiator can only provide about 40 % of the necessary full load heat rejection. In addition, the increased complexity and thermal load of integrating the braking resistor in the FC cooling loop has been evaluated, showing that the vehicle performance is not only thermally limited during uphill but also downhill driving.

The presented model is a platform not only suited to evaluate thermal management solutions but also to investigate refined FC models, energy management strategies or component sizing. Despite the focus on HD trucks, the scalable and modular vehicle and FCS model can be adapted for different high-power FC applications like planes, trains or ships.

Declaration of competing interest

The authors declare that they have no known competing financial interests or personal relationships that could have appeared to influence the work reported in this paper.

Acknowledgment

The Competence Centre TechForH2 is hosted by Chalmers University of Technology and is financially supported by the Swedish Energy Agency (P2021-90268) and the member companies Volvo, Scania, Siemens Energy, GKN Aerospace, PowerCell, Oxeon, RISE, Stena Rederier AB, Johnson Matthey and Insplorion.

The authors would like to thank Gustavo Hindi from Volvo Trucks for the support on the vehicle model parametrization and verification.

Data availability

The data that has been used is confidential.

References

[1] Reducing CO_2 emissions from heavy-duty vehicles - European Commission. Accessed: Jul. 09, 2024. [Online]. https://climate.ec.europa.eu/eu-action/transport/road-transport-reducing-co2-emissions-vehicles/reducing-co2-emissions-heavy-duty-vehicles_en.

[2] R.P. O'Hayre, S.-W. Cha, W.G. Colella, F.B. Prinz, *Fuel Cell Fundamentals*, third ed., John Wiley & Sons Inc, Hoboken, New Jersey, 2016.

[3] G. Zhang, S.G. Kandlikar, A critical review of cooling techniques in proton exchange membrane fuel cell stacks, Int. J. Hydrog. Energy. 37 (3) (2012), https://doi.org/10.1016/j.ijhydene.2011.11.010.

[4] D.A. Cullen, et al., New roads and challenges for fuel cells in heavy-duty transportation, Nat. Energy 6 (5) (2021) 5, https://doi.org/10.1038/s41560-021-00775-z.

[5] S. Pardhi, S. Chakraborty, D.-D. Tran, M. El Baghdadi, S. Wilkins, O. Hegazy, A review of fuel cell powertrains for long-haul heavy-duty vehicles: technology, hydrogen, energy and thermal management solutions, Energies 15 (24) (2022) 24, https://doi.org/10.3390/en15249557.

[6] M. Pihlatie, M. Ranta, P. Rahkola, R. Åman, Zero-emission truck powertrains for regional and long-haul missions, World Electr. Veh. J. 14 (9) (2023) 9, https://doi.org/10.3390/wevj14090253.

[7] K. Jiao, et al., Designing the next generation of proton-exchange membrane fuel cells, Nature. 595 (7867) (2021) 7867, https://doi.org/10.1038/s41586-021-03482-7.

[8] K. Mayr et al., Systemvergleich zwischen Wasserstoffverbrennungsmotor und Brennstoffzelle im schweren Nutzfahrzeug. *E-Mobil BW GmbH – Landesagentur Für Neue Mobilitätslösungen Automot. Baden-Württ. Stuttg.*, 2021, [Online]. https://www.e-mobilbw.de/fileadmin/media/e-mobilbw/Publikationen/Studien/e-mobilBW-Studie_H2-Systemvergleich.pdf.

[9] C. Doppler, B. Lindner-Rabl, Fuel cell trucks: thermal challenges in heat exchanger layout, Energies 16 (10) (2023) 10, https://doi.org/10.3390/en16104024.

[10] J. Linderl, J. Mayr, M. Hütter, R. Döbereiner, Optimized fuel cell drive for long-haul trucks, Atzheavy Duty Worldw. 14 (1) (2021) 38–43, https://doi.org/10.1007/s41321-021-0407-5.

[11] J. Marcinkoski, R. Vijayagopal, J. Adams, B. James, J. Kopasz, R. Ahluwalia. Hydrogen Class 8 Long Haul Truck Targets (US Department of Energy). 2019, [Online]. https://www.hydrogen.energy.gov/ pdfs/19006_hydrogen_class8_long_haul_truck_targets.pdf.

[12] Volvo Trucks showcases new zero-emissions truck. Accessed: Jul. 26, 2024. [Online]. https://www.volvotrucks.com/en-en/news-stories/press-releases/2022/jun/volvo-trucks-showcases-new-zero-emissions-truck.html.

[13] Daimler Truck #HydrogenRecordRun: Mercedes-Benz GenH2 Truck cracks 1,000 kilometer mark with one fill of liquid hydrogen. Accessed: Jul. 26, 2024. [Online]. https://www.daimlertruck.com/en/newsroom/pressrelease/daimler-truck-hydr

ogenrecordrun-mercedes-benz-genh2-truck-cracks-1000-kilometer-mark-with-one-fill-of-liquid-hydrogen-52369346.
[14] XCIENT Fuel Cell | HYUNDAI Truck & Bus. Accessed: Oct. 21, 2022. [Online]. https://trucknbus.hyundai.com/global/en/products/truck/xcient-fuel-cell.
[15] TOYOTA fuel cells | Applications. Accessed: Jul. 26, 2024. [Online]. https://www.toyota.co.jp/fuelcells/en/applications.html.
[16] TRE FCEV - Nikola Hydrogen Fuel Cell Electric Vehicle. Accessed: Jul. 26, 2024. https://www.nikolamotor.com/tre-fcev.
[17] Hydrogen Electric Fuel Cell Solutions | PowerCell Group. Accessed: Jul. 26, 2024. https://powercellgroup.com/.
[18] cellcentric – A Daimler Truck & Volvo Group Company. Accessed: Jul. 26, 2024. https://cellcentric.net/en/.
[19] Fuel Cell & Clean Energy Solutions | Ballard Power. Accessed: Jul. 26, 2024. https://www.ballard.com/.
[20] Symbio. Accessed: Oct. 21, 2022. [Online]. https://www.symbio.one/en/#!.
[21] 2025 Toyota Mirai | Toyota.com. Accessed: May 05, 2025. [Online]. https://www.toyota.com/mirai/.
[22] Y. Nonobe, Development of the fuel cell vehicle mirai, IEEJ Trans. Electr. Electron. Eng. 12 (1) (2017) 1, https://doi.org/10.1002/tee.22328.
[23] H. Lohse-Busch, et al., Automotive fuel cell stack and system efficiency and fuel consumption based on vehicle testing on a chassis dynamometer at minus 18 °C to positive 35 °C temperatures, Int. J. Hydrog. Energy. 45 (1) (2020) 861–872, https://doi.org/10.1016/j.ijhydene.2019.10.150.
[24] NEXO. Hyundai. Accessed: May 05, 2025. [Online]. https://www.hyundai.com/eu/models/nexo.html.
[25] J. Sery, P. Leduc, Fuel cell behavior and energy balance on board a Hyundai Nexo, Int. J. Engine Res. 23 (5) (2022) 5, https://doi.org/10.1177/14680874211059046.
[26] S. Tanaka, K. Nagumo, M. Yamamoto, H. Chiba, K. Yoshida, R. Okano, Fuel cell system for honda CLARITY fuel cell, eTransportation 3 (2020) 100046, https://doi.org/10.1016/j.etran.2020.100046.
[27] E. Alpaslan, et al., A review on fuel cell electric vehicle powertrain modeling and simulation, Energy Sourc. Part Rec. Util. Environ. Eff. (2021) 1–37, https://doi.org/10.1080/15567036.2021.1999347.
[28] P.H. Affonso Nóbrega, A review of physics-based low-temperature proton-exchange membrane fuel cell models for system-level water and thermal management studies, J. Power Sources 558 (2023) 232585, https://doi.org/10.1016/j.jpowsour.2022.232585.
[29] T. Jahnke, et al., Performance and degradation of proton exchange membrane fuel cells: state of the art in modeling from atomistic to system scale, J. Power Sources 304 (2016) 207–233, https://doi.org/10.1016/j.jpowsour.2015.11.041.
[30] Y. Wang, X. Yang, Z. Sun, Z. Chen, A systematic review of system modeling and control strategy of proton exchange membrane fuel cell, Energy Rev. 3 (1) (2024) 1, https://doi.org/10.1016/j.enrev.2023.100054.
[31] J. T. Pukrushpan, A. G. Stefanopoulou, H. Peng, Control of fuel cell power systems, in: Advances in Industrial Control, Springer London, London, 2004. doi: 10.1007/978-1-4471-3792-4.
[32] R.K. Ahluwalia, X. Wang, Performance and durability of hybrid fuel cell systems for class-8 long haul trucks, J. Electrochem. Soc. 171 (3) (2024) 3, https://doi.org/10.1149/1945-7111/ad300f.
[33] S. Paul, D. Fnu, S. Joshi, M. Franke, D. Tomazic, Model-based approach for optimization of propulsion system of a heavy-duty class 8 fuel cell electric vehicle. Presented at the WCX SAE World Congress Experience, Detroit, Michigan, United States. 2024, pp. 2024-01–2167. doi: 10.4271/2024-01-2167.
[34] C. Geng, S. Mei, L. Liu, W. Ma, Q. Xue, Simulation and experimental research on energy management control strategy for fuel cell heavy-duty truck, Int. J. Hydrog. Energy. 69 (2024) 1305–1318, https://doi.org/10.1016/j.ijhydene.2024.05.081.
[35] M. Wagenblast, et al., Design and analysis of a spray cooling system for a heavy-duty fuel cell truck, pp. 2022–01–5054, SAE Tech. Pap. (2022), https://doi.org/10.4271/2022-01-5054.
[36] E. Weiss, S. Schnorpfeil, D. Nickel, Fuel cell system integration for heavy-duty applications, in: *Heavy-Duty-, On- und Off-Highway-Motoren 2021*, J. Liebl, Ed., in Proceedings. Wiesbaden: Springer Fachmedien Wiesbaden. 2022. 219–229. doi: 10.1007/978-3-658-38105-9_16.
[37] R. Döbereiner, R. Steinek, AVL Fuel Cell Truck Presentation. 2024. Accessed: May 05, 2025. [Online]. https://www.avl.com/sites/default/files/2024-05/en_presentation_avl_fuel_cell_truck_05.24.pdf.
[38] J. Pell, C. Schörghuber, S. Pretsch, H. Schreier, Optimized operating strategies for fuel cell trucks, Atzheavy Duty Worldw. 15 (1) (2022) 1, https://doi.org/10.1007/s41321-021-0464-9.
[39] J. Pell, C. Schörghuber, T. Schubert, S. Ozli, Energy and lifetime management for fuel cell powered trucks, Atzheavy Duty Worldw. 13 (4) (2020) 4, https://doi.org/10.1007/s41321-020-0110-y.
[40] T. Fürnhammer, R. Döbereiner, F. Bayer, Trucks with fuel cell technology - leading-edge solutions, Atzheavy Duty Worldw. 16 (2) (2023) 2, https://doi.org/10.1007/s41321-023-1027-z.
[41] Q. Li, W. Chen, Z. Liu, M. Li, L. Ma, Development of energy management system based on a power sharing strategy for a fuel cell-battery-supercapacitor hybrid tramway, J. Power Sources 279 (2015) 267–280, https://doi.org/10.1016/j.jpowsour.2014.12.042.
[42] F. Peng, W. Chen, Z. Liu, Q. Li, C. Dai, System integration of China's first proton exchange membrane fuel cell locomotive, Int. J. Hydrog. Energy. 39 (25) (2014) 25, https://doi.org/10.1016/j.ijhydene.2014.01.166.
[43] P. Garcia, L.M. Fernandez, C.A. Garcia, F. Jurado, Fuel cell-battery hybrid system for transport applications, in: *2009 International Conference on Electrical Machines and Systems*, IEEE, Tokyo, Japan, 2009, pp. 1–5, https://doi.org/10.1109/ICEMS.2009.5382685.
[44] P. García, J.P. Torreglosa, L.M. Fernández, F. Jurado, Viability study of a FC-battery-SC tramway controlled by equivalent consumption minimization strategy, Int. J. Hydrog. Energy. 37 (11) (2012) 11, https://doi.org/10.1016/j.ijhydene.2012.02.184.
[45] M. Schröder, F. Becker, C. Gentner, Optimal design of proton exchange membrane fuel cell systems for regional aircraft, Energy Convers. Manag. 308 (May 2024) 118338, https://doi.org/10.1016/j.enconman.2024.118338.
[46] M. Schröder, F. Becker, J. Kallo, C. Gentner, Optimal operating conditions of PEM fuel cells in commercial aircraft, Int. J. Hydrog. Energy. 46 (66) (2021) 66, https://doi.org/10.1016/j.ijhydene.2021.07.099.
[47] M. Chiara Massaro, S. Pramotton, P. Marocco, A.H.A. Monteverde, M. Santarelli, Optimal design of a hydrogen-powered fuel cell system for aircraft applications, Energy Convers. Manag. 306 (2024) 118266, https://doi.org/10.1016/j.enconman.2024.118266.
[48] C. Mayer, J. Karner, T. Eberhart, K. Huber, J. Konrad, Fuel cell electric tractor FCTRAC: vehicle design and architecture, Agric. Eng. 79 (3) (2024) 3, https://doi.org/10.15150/AE.2024.3315.
[49] J. Konrad, C. Varlese, R. Krizan, C. Junger, P. Hofmann, C. Mayer, Fuel cell electric tractor FCTRAC: powertrain, thermal system, hydrogen storage, and performance, Agric. Eng. 79 (3) (2024) 3, https://doi.org/10.15150/AE.2024.3314.
[50] F. Breuer, P. Philipp, L. Frerichs, Rule-based energy management strategy for a fuel cell long-haul truck, pp. 2022–01–5070, SAE Tech. Pap. (2022), https://doi.org/10.4271/2022-01-5070.
[51] E.G. Amaya, H.G. Chiacchiarini, C.D. Angelo, Energy managment system designed for reducing operational costs of a hybrid fuel cell-battery-ultracapacitor vehicle, in: *2020 IEEE Vehicle Power and Propulsion Conference (VPPC)*, IEEE, Gijon, Spain, 2020, pp. 1–5, https://doi.org/10.1109/VPPC49601.2020.9330889.
[52] A. Ferrara, S. Jakubek, C. Hametner, Energy management of heavy-duty fuel cell vehicles in real-world driving scenarios: Robust design of strategies to maximize the hydrogen economy and system lifetime, Energy Convers. Manag. 232 (2021) 113795, https://doi.org/10.1016/j.enconman.2020.113795.
[53] C. Boßer, D. Sedarsky, Bubble column evaporative cooling for pemfc thermal management in heavy-duty vehicles, in: Presented at the 10th Thermal and Fluids Engineering Conference (TFEC), Begel House Inc., 2025, https://doi.org/10.1615/TFEC2025.mes.055991.
[54] D. K. Lee, D. S. Kim, H. S. Byun, H. S. Kang, Y. H. Shin, H. S. Lee, maximizing FCEV stack cooling performance: developing a performance prediction model based on machine learning for evaporative cooling radiator, Presented at the WCX SAE World Congress Experience, Detroit, Michigan, United States, 2024, pp. 2024-01–2586. doi: 10.4271/2024-01-2586.
[55] R. Prabakaran, M. Mohamed Souby, J. Liu, S. Chul Kim, Thermal performance of a stack cooling radiator coupled with spray cooling for the future fuel cell electric vehicles, Appl. Therm. Eng. 246 (2024) 122975, https://doi.org/10.1016/j.applthermaleng.2024.122975.
[56] E. Torenbeek, *Advanced Aircraft Design: Conceptual Design, Analysis and Optimization of Subsonic Civil Airplanes*, 1st ed., Wiley, 2013, 10.1002/9781118568101.
[57] "Fuel Cell Systems for Heavy Commercial Vehicles. cellcentric. Accessed: May 06, 2025. [Online]. https://www.cellcentric.net/en-us/technology-bza150.
[58] N. Marx, L. Boulon, F. Gustin, D. Hissel, K. Agbossou, A review of multi-stack and modular fuel cell systems: Interests, application areas and on-going research activities, Int. J. Hydrog. Energy. 39 (23) (2014) 23, https://doi.org/10.1016/j.ijhydene.2014.05.187.
[59] A.L. Dicks, D.A.J. Rand, *Fuel Cell Systems Explained (3rd Edition)*, John Wiley & Sons, 2018.
[60] S. Yu, D. Jung, Thermal management strategy for a proton exchange membrane fuel cell system with a large active cell area, Renew. Energy 33 (12) (2008) 12, https://doi.org/10.1016/j.renene.2008.02.015.
[61] F.P. Incropera, D.P. DeWitt, T.L. Bergman, A.S. Lavine (Eds.), *Fundamentals of Heat and Mass Transfer*, 6 ed., Wiley, Hoboken, NJ, 2007.
[62] S. Schnorpfeil, A. Kotowski, H. Sötje, G. Hartmann, Fuel cell system development for heavy duty application, in: A. Heintzel (Ed.), *Heavy-Duty-, On- und Off-Highway-Motoren 2022*, in Proceedings, Springer Fachmedien Wiesbaden, Wiesbaden. 2023. 172–183. doi: 10.1007/978-3-658-41477-1_14.
[63] ENTARON FC 13 High Efficiency Filter System - Variant 1. MANN+HUMMEL, datasheet. Accessed: May 06, 2025. [Online]. https://shop.mann-hummel.com/en/e-mobility/entaron-fc-7-5-filter-system-2.html.
[64] Rotrex Fuel Cell compressors. Rotrex, datasheet. Accessed: Apr. 08, 2025. [Online]. https://rotrex-fuel-cell-compressor.com/fuel-cell-compressors/.
[65] J. Hanschke, S. Schmalzriedt, Verfahren zur Druckregelung - Daimler AG, 70327, Stuttgart, DE. DE 10 2013 014 413 A1, 2013 [Online]. https://depatisnet.dpma.de/DepatisNet/depatisnet?action=pdf&docid=DE102013014413A1&xxxfull=1.
[66] A. Hansson, M. Abu Al-Soud, Turbo for Fuel Cell Electric Vehicle. Thesis for the degree of Master of Science, Lund University, Volvo Powertrain AB, Lund, Sweden, 2022. [Online]. http://lup.lub.lu.se/student-papers/record/9084918.
[67] FCmove®-XD. Ballard, datasheet. Accessed: May 06, 2025. https://www.ballard.com/wp-content/uploads/2024/11/Ballard-Data-Sheet-FCmove-XDv2_20250305_landscape-2.pdf.
[68] F. Barbir, PEM Fuel Cells: Theory and Practice, 2nd ed., Elsevier/Academic Press, Amsterdam; Boston, 2013.
[69] SRM ARC-17. Svenska Rotor Maskiner SRM, datasheet. Accessed: May 06, 2025. [Online]. https://rotor.se/wp-content/uploads/2020/02/Datasheet-ARC.pdf.
[70] Questions and Answers on Weights and Dimensions. European Commission - European Commission. Accessed: Jul. 17, 2024. [Online]. https://ec.europa.eu/commission/presscorner/detail/en/qanda_23_3770.

[71] L. Guzzella, A. Sciarretta, Vehicle Propulsion Systems: Introduction to Modeling and Optimization, Springer, Berlin Heidelberg, 2013 doi: 10.1007/978-3-642-35913-2.
[72] K. Popp, W. Schiehlen, Ground Vehicle Dynamics, Springer, Berlin Heidelberg, 2010, 10.1007/978-3-540-68553-1.
[73] Factsheet - Volvo electric drive unit. Volvo Trucks, datasheet. Accessed: May 06, 2025. https://stpi.it.volvo.com/STPIFiles/Volvo/FactSheet/EPT2412_Eng_01_332277022.pdf.
[74] Daimler Trucks presents technology strategy for electrification – world premiere of Mercedes-Benz fuel-cell concept truck. Daimler Truck AG. Accessed: Apr. 30, 2024. https://www.daimlertruck.com/en/newsroom/pressrelease/daimler-trucks-presents-technology-strategy-for-electrification-world-premiere-of-mercedes-benz-fuel-cell-concept-truck-47453560.
[75] S. Yun, J. Yun, J. Han, Development of a 470-horsepower fuel cell-battery hybrid Xcient dynamic model using SimscapeTM, Energies 16 (24) (2023), https://doi.org/10.3390/en16248092.
[76] A. Ramesh Babu, J. Andric, B. Minovski, S. Sebben, System-level modeling and thermal simulations of large battery packs for electric trucks, Energies 14 (16) (2021), https://doi.org/10.3390/en14164796.
[77] T. Rudolf, T. Schurmann, S. Schwab, S. Hohmann, Toward holistic energy management strategies for fuel cell hybrid electric vehicles in heavy-duty applications, Proc. IEEE 109 (6) (2021), https://doi.org/10.1109/JPROC.2021.3055136.
[78] WHBSA. Danotherm, datasheet. Accessed: May 06, 2025. [Online]. https://www.danotherm.com/download/18.1e8fb7dd17f7bc35ec6d712/1648129324697/WHBSA.pdf.
[79] A. Khalatbarisoltani, H. Zhou, X. Tang, M. Kandidayeni, L. Boulon, X. Hu, Energy management strategies for fuel cell vehicles: a comprehensive review of the latest progress in modeling, strategies, and future prospects, IEEE Trans. Intell. Transp. Syst. 25 (1) (2024), https://doi.org/10.1109/TITS.2023.3309052.
[80] Vehicle Energy Consumption calculation TOol - VECTO. European Commission. Accessed: Aug. 15, 2024. https://climate.ec.europa.eu/eu-action/transport/road-transport-reducing-co2-emissions-vehicles/vehicle-energy-consumption-calculation-tool-vecto_en.
[81] G. Moratti, M. Villani, D. Beltrami, S. Uberti, P. Iora, L. Tribioli, Optimization with dynamic programming of the energy management strategy for a fuel cell hybrid heavy-duty truck minimizing hydrogen consumption and degradation, Presented at the Conference on Sustainable Mobility, Catania, Italy. 2024, pp. 2024-24–0004. doi: 10.4271/2024-24-0004.
[82] OmniFlow i6-3. MANN+HUMMEL, datasheet. Accessed: May 07, 2025. https://shop.mann-hummel.com/en/e-mobility/omniflow-i6-3-e.html.
[83] WP150 HV. EMP, datasheet. Accessed: Nov. 12, 2024. [Online]. https://www.emp-corp.com/product/wp150-high-voltage/.
[84] L. Yang, N.-N. Nik-Ghazali, M.A.H. Ali, W.T. Chong, Z. Yang, H. Liu, A review on thermal management in proton exchange membrane fuel cells: Temperature distribution and control, Renew. Sustain. Energy Rev. 187 (2023) 113737, https://doi.org/10.1016/j.rser.2023.113737.
[85] M. Nöst, C. Doppler, M. Klell, A. Trattner, Chapter 7 - thermal management of PEM fuel cells in electric vehicles, in: D. Watzenig and B. Brandstätter (Eds.), *Comprehensive Energy Management - Safe Adaptation, Predictive Control and Thermal Management*, SpringerBriefs in Applied Sciences and Technology, Graz, Austria: Springer International Publishing, 2018, pp. 102–121. doi: 10.1007/978-3-319-57445-5.
[86] S. Yu, D. Jung, A study of operation strategy of cooling module with dynamic fuel cell system model for transportation application, Renew. Energy 35 (11) (2010) 11, https://doi.org/10.1016/j.renene.2010.03.023.
[87] Y.A. Cengel, J.M. Cimbala, F. Mechanics, *Fundamental and Application*, fourth ed., McGraw-Hill, New York, 2018.
[88] FiC-15 HV Fan. EMP, datasheet. Accessed: May 07, 2025. [Online]. https://www.emp-corp.com/product/15-inch-high-voltage-fan/.
[89] B. Sundén, Hydrogen, batteries and fuel cells, in: *Hydrogen, Batteries and Fuel Cells*, Elsevier, 2019, pp. 15–36, https://doi.org/10.1016/B978-0-12-816950-6.00002-6.
[90] J. F. Hellmuth, M. M. Steeb, M. Pollak, F. Jäger, W. Tegethoff, J. Köhler, Innovative thermal management operating strategies for battery-electric heavy-duty trucks, in: 36th International Conference on Efficiency, Cost, Optimization, Simulation and Environmental Impact of Energy Systems (ECOS 2023), Las Palmas De Gran Canaria, Spain: ECOS 2023, 2023, pp. 2581–2592. doi: 10.52202/069564-0232.
[91] P. Reithuber, C. Frühwirth, S. Buchberger, H. Eichlseder, Investigation of the proton exchange membrane fuel cell system cathode exhaust gas composition based on test bed measurements, Energies 16 (16) (2023) 6057, https://doi.org/10.3390/en16166057.
[92] VOLVO D13 engine family. Volvo Trucks, datasheet. Accessed: May 07, 2025. [Online]. https://www.volvotrucks.us/media/vtna/files/shared/powertrain/revised4147-101-volvo-d13-engine-brochure-low-res.pdf.
[93] Factsheet engine brake. Volvo Trucks, datasheet. Accessed: May 07, 2025. [Online]. https://stpi.it.volvo.com/STPIFiles/Volvo/FactSheet/EBR-VEB+,EBR-VEB,EBR-EPG,EBR-EPGC_Eng_01_331737334.pdf.
[94] Institution of Mechanical Engineers - IMechE, Advanced Thermal Management in Future Hydrogen Fuel Cell Powered Vehicles, (Jun. 13, 2021). Accessed: Jan. 13, 2023. [Online Video]. https://www.youtube.com/watch?v=wol9w7qqKmI.